AFOSR FINAL REPORT

Principal Investigator:

Dr. Miao Yu
Associate Professor
Department of Mechanical Engineering
University of Maryland
College Park, MD 20742
mmyu@umd.edu
Tel: 301-405-3591

Project Title:

Fly Ear Inspired Miniature Acoustic Sensors for Detection and Localization

Grant No:

FA9550-08-1-0042

Period of Performance:

2/1/2008-4/30/2011

REPORT DOCUMENTATION PAGE

Form Approved
OMB No. 0704-0188

1. REPORT DATE *(DD-MM-YYYY)*	2. REPORT TYPE	3. DATES COVERED *(From - To)*
7/31/2011	Final Report	2/1/2008-4/30/2011

4. TITLE AND SUBTITLE
Fly-Ear Inspired Miniature Acoustic Sensors for Target Detection and Localization

5a. CONTRACT NUMBER

5b. GRANT NUMBER
FA95500810042

5c. PROGRAM ELEMENT NUMBER

6. AUTHOR(S)
Miao Yu

5d. PROJECT NUMBER

5e. TASK NUMBER

5f. WORK UNIT NUMBER

7. PERFORMING ORGANIZATION NAME(S) AND ADDRESS(ES)

University of Maryland
College Park, MD 20742

8. PERFORMING ORGANIZATION REPORT NUMBER

9. SPONSORING / MONITORING AGENCY NAME(S) AND ADDRESS(ES)
Dr. Willard Larkin
Air Force Office of Scientific
Directorate of Mathematics, Information, and Life Science
875 North Randolph St
Arlington, VA 22203-1768

10. SPONSOR/MONITOR'S ACRONYM(S)
AFOSR

11. SPONSOR/MONITOR'S REPORT NUMBER(S)
AFRL-OSR-VA-TR-2012-0206

12. DISTRIBUTION / AVAILABILITY STATEMENT

A

13. SUPPLEMENTARY NOTES

14. ABSTRACT
Inspired by the micro-scale ears of the fly Ormia, which show remarkable sound localization ability, the overall objective of this project is to achieve a further understanding of the mechanism the fly ear and use this understanding to develop Fly-Ear Inspired Miniature Acoustic Sensors for Target Detection and Localization. Through mechanics and optimization analysis, we have discovered an important biological conclusion: the fly ear can be viewed as a nature-designed optimal structure that is endowed with the dual optimality characteristic. A micro-scale fly-ear inspired directional microphone has been developed to fully capture the dual optimality characteristic of the fly ear. Furthermore, a localization strategy inspired by the fly's localization/lateralization scheme has been employed. It has also been found that not only the fly ear represents a nature designed optimal structure; the fly's localization scheme may also resemble an optimal control scheme. This work can form a basis to unravel the underlying science of fly-ear mechanisms and provide a framework for the development of bio-inspired localization, tracking, and navigation systems.

15. SUBJECT TERMS
Fly ear, bio-inspired sensor, microphone, directional cues, sound localization

16. SECURITY CLASSIFICATION OF:			17. LIMITATION OF ABSTRACT	18. NUMBER OF PAGES	19a. NAME OF RESPONSIBLE PERSON
a. REPORT	**b. ABSTRACT**	**c. THIS PAGE**		23	Miao Yu
					19b. TELEPHONE NUMBER *(include area code)* 301 405 3591

Standard Form 298 (Rev. 8-98)
Prescribed by ANSI Std. Z39.18

I. Introduction

Animal hearing organs are governed by a fundamental size constraint; the smaller the organ size, the smaller the available directional cues for directional hearing. However, with an auditory organ separation of only 520 μm, it is remarkable that the parasitic fly *Ormia ochracea* can achieve a human-like localization precision. The key to this fly's phenomenal directional hearing ability is believed to be due to the mechanical coupling between its two eardrums. The overall goal of this AFOSR sponsored research program is to achieve a fundamental understanding of the mechanism the fly ear and use this understanding to develop fly-ear inspired miniature acoustic sensors for target detection and localization. Over the three-year research program, significant progresses have been made toward achieving this goal. First, through mechanics and optimization analysis, we have discovered an important biological conclusion: the fly ear can be viewed as a nature-designed optimal structure that is endowed with the dual optimality characteristic: maximum average directional sensitivity and minimum nonlinearity over the azimuth range of -30 degrees to 30 degrees achieved simultaneously at the fly ear's working frequency of 5 kHz. Furthermore, a micro-scale fly-ear inspired directional microphone has been developed to fully capture the dual optimality characteristic of the fly ear. A lab-on-a-chip optical detection system has also been developed to realize a fully integrated and miniaturized sensor system. Moreover, a localization strategy inspired by the fly's localization/lateralization scheme has been developed and employed experimentally. In addition, it has also been found that not only the fly ear represents a nature designed optimal structure; the fly's localization scheme may also resemble an optimal control scheme. This work can form a basis to unravel the underlying science of fly-ear mechanisms and provide a framework for the development of bio-inspired localization, tracking, and navigation systems.

II. Technical Summary of Accomplishments

A. Fundamental understanding of the fly's dual optimality characteristics

In this project, we have furthered the understanding of fly-ear mechanisms and used this understanding to develop fly-ear inspired sensors. We have found the answers to the following fundamental questions: i) how have the structural parameters of the fly ears been tailored for achieving its superior localization ability at 5 kHz, ii) does the fly ear represent a nature-designed optimal structure to facilitate the fly's unique localization-lateralization scheme, and iii) can a synthetic device be developed to truly replicate the fly-ear characteristics.

The mechanics model used in this study is an equivalent two-degree-of-freedom model along with its relevant parameters (Miles et al, 1995[1]). As shown in Figure 1, the two tympana are modeled as two rigid bars connected by a torsion spring k_3. The outer end of each bar is supported by a translational spring k_1 or k_2, which is equivalent to the tympanum stiffness. Dashpots c_1, c_2 and c_3 are added to account for the damping ratios of the system. All the parameters used to study the fly ear structure are listed in Table 1.
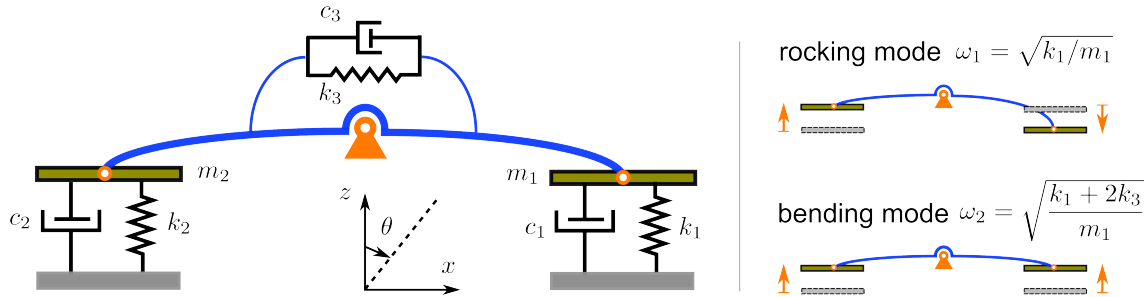

Figure 1: Equivalent 2-DOF model of the fly ear.

The governing equations of the coupled system can be obtained as follows:

$$\mathbf{M}\begin{Bmatrix}\ddot{x}_1\\\ddot{x}_2\end{Bmatrix}+\mathbf{C}\begin{Bmatrix}\dot{x}_1\\\dot{x}_2\end{Bmatrix}+\mathbf{K}\begin{Bmatrix}x_1\\x_2\end{Bmatrix}=\begin{Bmatrix}F_1\\F_2\end{Bmatrix},\tag{1}$$

where

$$\mathbf{M}=\begin{bmatrix}m&\\&m\end{bmatrix},\mathbf{C}=\begin{bmatrix}c_1+c_3&c_3\\c_3&c_1+c_3\end{bmatrix},\mathbf{K}=\begin{bmatrix}k_1+k_3&k_3\\k_3&k_1+k_3\end{bmatrix}.\tag{2}$$

Table 1: Parameters used in the 2-DOF model for the fly ear (Miles, et al., 1995)

Parameters	Values
Mass of bar m	2.88×10^{-10} kg
Translational spring k_1,k_2	0.576 N/m
Translation dashpot c_1,c_2	1.15×10^{-5} N s/m
Torsional spring k_3	5.18 N/m
Torsional dashpot c_3	2.88×10^{-5} N s/m
Separation of force locations d	1.2×10^{-3} m
Tympanum area s	0.288×10^{-6} m^2
Excitation frequency ω	3.14×10^{4} rad/s (5 kHz)
Sound speed c	344 m/s

In the case of free vibration, the natural frequencies and mode shapes of the system can be found as:

$$\omega_1=\sqrt{k_1/m},\omega_2=\sqrt{(k_1+2k_2)/m},\tag{3}$$

$$\mathbf{v}_1=\begin{bmatrix}-1&1\end{bmatrix}^T,\mathbf{v}_2=\begin{bmatrix}1&1\end{bmatrix}^T,\tag{4}$$

where the two diaphragms move out of phase in the first mode (rocking mode), and in phase in the second mode (bending mode).

Following an approach different from that used in the existing literature, modal analysis is carried out and this allows us to obtain analytical solutions for the directional cues of the fly ear and understand how the structural parameters of the fly ear affect its performance. By using modal analysis[2], the responses to an acoustic stimulus $p_0e^{j\omega t}$ (p_0 is the pressure reference on the midline) are obtained as

$$\begin{Bmatrix}x_1\\x_2\end{Bmatrix}=\begin{Bmatrix}A_1\\A_2\end{Bmatrix}e^{j\omega t}=\frac{p_0s}{k_1}\frac{\cos\phi}{1-\Omega^2+j2\xi_1\Omega}\begin{Bmatrix}\Gamma+j\tan(\phi/2)\\\Gamma-j\tan(\phi/2)\end{Bmatrix},\tag{5}$$

where

$$\Gamma=\frac{1-\Omega^2+j2\xi_1\Omega}{\eta^2-\Omega^2+j2\eta\xi_2\Omega},\phi=2\pi\chi\sin\theta,\chi=\frac{d}{\lambda},\tag{6}$$

$$\Omega=\omega/\omega_1,\eta=\omega_2/\omega_1,\xi_1=c_1/(2\omega_1 m),\xi_2=(c_1+2c_3)/(2\omega_2 m).\tag{7}$$

Here, Γ represents the relative contribution of the two modes subject to unit modal force, which is dependent on the natural frequency ratio η, the damping factors $\xi_{1,2}$, and the normalized excitation

frequency Ω. ϕ represents the phase difference of the incident sound field applied to the two mass-spring systems.

Then, mechanical interaural intensity difference (mIID) and mechanical interaural phase difference (mIPD) between the two eardrums can be analytically obtained as

$$mIID = 20\log_{10}\left|\frac{A_1}{A_2}\right|, \tag{8}$$

$$mIPD = \angle\frac{A_1}{A_2} = \angle\frac{\Gamma + j\tan(\phi/2)}{\Gamma - j\tan(\phi/2)}. \tag{9}$$

Equivalent to *mITD*, the mechanical interaural phase difference (*mIPD*) is chosen as the directional cue for investigation, since it is a dimensionless measure that is independent of the sound wavelength and sound speed.

On the midline ($\theta = 0$), both mIID and mIPD are equal to zero. In our study, mIPD is chosen as the main directional cue, for which the directional sensitivity (DS) is defined as the first derivative of mIPD with respect to azimuth:

$$DS = \partial mIPD/\partial\theta. \tag{10}$$

It is worth noting that the localization performance does not only depend on the absolute value of *mIPD*, but more importantly, it is the directional sensitivity, that determines how accurately the fly can pinpoint a source.

Based on the analytical solutions of *mIPD* and *DS*, it is easy to see that *mIPD* and *DS* solely depend on two parameters: the modal response ratio Γ and the initial phase difference ϕ. The former relates to the resonance frequency ratio η (the ratio of the bending mode natural frequency ω_2 to the rocking mode natural frequency ω_1), normalized working frequency Ω (the ratio of the sound-source frequency to the rocking mode natural frequency), and damping ratios ξ_1 and ξ_2. The latter relates to the separation-to-wavelength ratio χ (the ratio of the membrane center separation d to the sound-source wavelength λ) and the sound-source azimuth θ.

By looking at the directional sensitivity, as shown in **Figure 2**, we can find out that in the vicinity of midline (-30°≤θ≤30°), DS is not only very flat at the fly's working frequency 5kHz, but it is higher than what is achievable at any other frequency. In other words, if we use a straight line to approximate mIPD in the azimuth range -30°≤θ≤30°, the linearity is best at 5kHz, and the slope is maximal. The localization/lateralization scheme takes full advantage of the linear range so that the fly can accurately pinpoint the crickets.
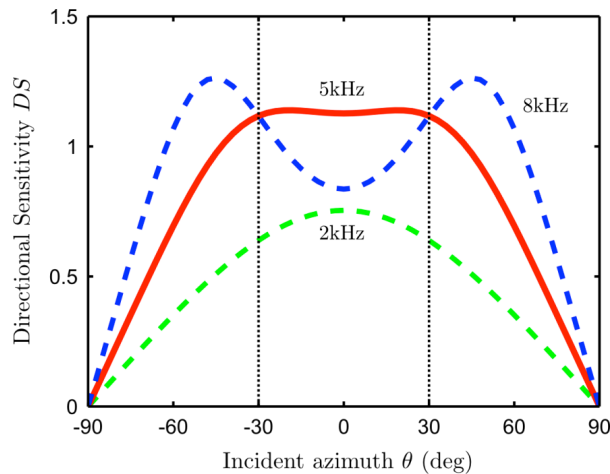

Figure 2: Directional sensitivity (DS) as a function of azimuth for various frequencies. 5kHz is the calling song frequency of the fly's host crickets.

Further, two performance metrics for further investigation can be defined: the nonlinearity (NL) of mIPD and the average DS (ADS) over the azimuth range of -30° to 30°. When these two metrics of the fly ear are plotted in the frequency domain in **Figure 3**, we are able to observe an interesting result: the minimum NL and the maximum ADS are achieved simultaneously at the frequency of 5kHz. This result suggests that the fly ear is endowed with a dual optimality characteristic at its working frequency.
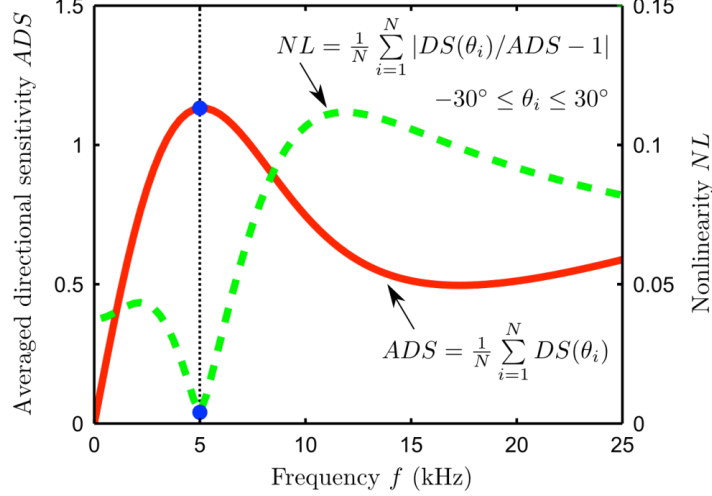

Figure 3: Directional sensitivity and nonlinearity of the fly ear in the frequency domain.

We further explore as to how the structural parameters of the fly ear are tailored to achieve such a dual optimality characteristic and whether a synthetic device endowed with the fly ear's dual optimality characteristic can be developed. An optimal design problem is formulated to seek solutions in the design space, which will meet the objective of achieving dual optimality (i.e., minimal NL and maximal ADS) over the azimuth of -30° to 30° at the same sound frequency (i.e., the optimal working frequency). For simplicity, the problem is constrained in one dimension (azimuth). Note that there are several key parameters, the resonance frequency ratio η, the separation-to-wavelength ratio χ, and the damping ratios that can influence the NL and ADS. In **Figure 4**, the rocking and bending mode natural frequencies that ensures the dual optimality characteristic are plotted as a function of separation-to-wavelength ratio χ for two damping scenarios: ξ_1=0.89 and ξ_2=1.23 for the fly ear case, and ξ_1 =0.17 and ξ_2 =0.05 for the other case. Given the fly-ear's geometric dimensions and its working frequency of 5kHz, following the two curves in **Figure 4**, the natural frequencies (rocking mode: 6.99kHz, bending mode: 30.1kHz) required to achieve the dual optimality can be obtained, which are found to be consistent with the experimental data reported in the literature (7.12kHz and 31.0kHz). This finding provides the evidence for the statement that the fly ear indeed represents a nature-designed optimal structure that can simultaneously achieve the maximum DS and the minimum NL at its working frequency of 5kHz.

Furthermore, to achieve such a dual optimality characteristic, proper contributions from both the rocking and the bending modes (i.e., resonance ratio η=4.36) are necessary. It is noted that the resonance ratio η is related the stiffness ratio $\sigma = k_3/k_1$ by $\eta^2=1+2\sigma$, which is the key non-dimensional structural parameter that determines how strongly the two ear membranes are coupled (i.e., the coupling strength). As shown in of **Figure 5**, given the same separation to wavelength ratio as the fly ear, if the coupling is weak (e.g., η=2), the amplification of phase difference is not significant, i.e., DS is too small to achieve the maximal value. On the other hand, when the coupling is rigid (e.g, η=20), even though the mIPD can be significantly amplified, it saturates at 180° when θ is slightly off the midline, and thus, it is not possible to distinguish the azimuths and the minimum NL is not achievable. Only when the coupling is "medium" (η=4.36), the fly ear can achieve a balance between DS and NL, and thus, the dual optimality can be achieved at its working frequency. This suggests that the structural parameters of the fly ear may

have been well adapted in the course of evolution, resulting in an appropriate coupling strength for achieving the dual optimality characteristic.
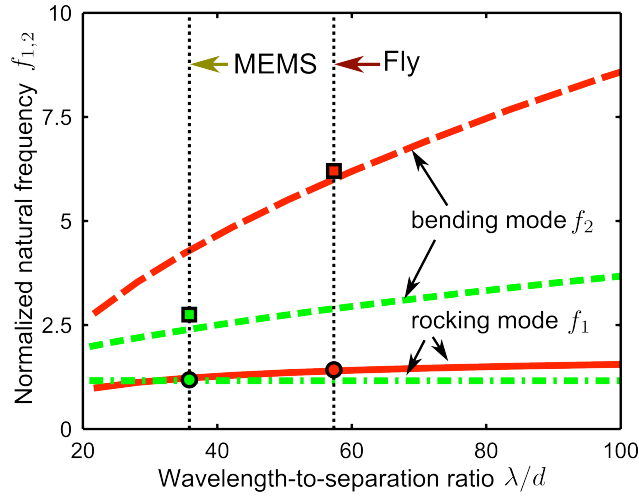

Figure 4: Design curves to achieve fly ear's dual optimality. Two damping scenarios are shown: ξ_1 = 0.89 and ξ_2 = 1.23 for the high damping case, and ξ_1 = 0.17 and ξ_2 = 0.05 for the low damping case. For any given wavelength-to-separation ratio in each case, the two natural frequencies for the rocking and bending modes can be obtained using the optimal design curves here, e.g. the fly ear in the high damping case, and the synthetic MEMS device in the low damping case.
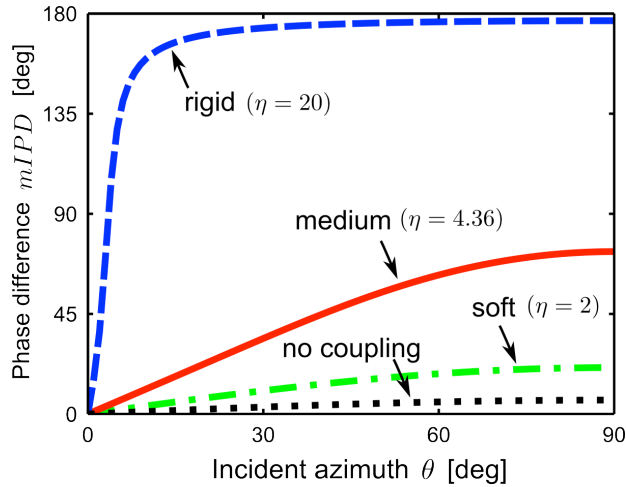

Figure 5: Phase difference with respect to incident azimuth for different coupling strength. In order to achieve dual-optimality, the coupling strength of the bridge (defined by the ratio of two natural frequencies) needs to be medium, neither too soft nor too rigid.

The dual optimality characteristic can provide a basis for understanding the fly's superior directional hearing capability as well as its unique localization-lateralization scheme. First, although the absolute value of the mIPD is maximal at the two extreme positions ($\theta=\pm90°$), the corresponding DS is close to zero at these positions and the maximal DS is actually achieved at the vicinity of the midline (θ =0°). Therefore, the fly naturally turns the head front (midline of the ear) towards the source so that the maximum DS (i.e., maximal slope) can be achieved to ensure the best localization precision. This is similar to a related finding reported for an Egypt fruit bat, which uses not the maximal sonar beam intensity but its maximal slope for target localization[3]. Second, mIPD is a linear function of azimuth in the range from -30° to 30°, which is coincident with the sigmoid relationship of fly's turning speed with

respect to the azimuth, obtained in the phonotactic experiments on the fly[4]. Given the limited neural processing ability of the fly, a linear and maximal DS can certainly help the fly perform the localization task more accurately and more efficiently for the azimuths from -30° to 30°. Therefore, in this sense, it is not only the mechanical coupling mechanism that helps the fly ear obtain significantly amplified directional cues, but more importantly, the structural parameters of the fly ear have been tailored to achieve the dual optimality characteristic at 5kHz, facilitating a unique localization-lateralization scheme for accurately pinpointing its host.

B. Development of Bio-Inspired Acoustic Sensor with Dual Optimality Characteristics

Inspired by the fly ear's dual optimality characteristics, fly-ear inspired sensors have been developed and experimentally demonstrated. The fly-ear inspired directional microphone consists of two clamped circular membranes (material: silicon, radius of 500 μm and thickness of 0.5 μm) and a coupling bridge (material: alternating SiO_2 and Si_3N_4 layers, size: 1250μm x300μmx3.2μm) that is pivoted in the middle and connects the two membrane centers. It is noted that the separation between diaphragm centers is designed to be 1.25 mm, same as that of the fly ear. The membrane structure is integrated with another layer of silicon, serving as holders for two optical fibers, which are used to detect the acoustic pressure induced membrane deflection. The bio-inspired MEMS directional microphone uses a low coherence fiber optic interferometer (LCFOI) system to detect the displacement of the two membrane centers. As shown in **Figure 6**, a superluminescent light emitting diode (SLED) is used as the broadband light source. The sensing interferometer is a Fabry-Pérot (FP) cavity formed between each membrane and the corresponding fiber tip as the sensing interferometer; the read-out interferometer is a fiber FP tunable filter (Micro Optics FFP-TF2). In order to achieve maximum sensitivity, biases are applied to the tunable filters to adjust the initial working position to be at quadrature points. Compared with conventional fiber optic interferometers, this detection system can substantially reduce the phase noise associated with light wavelength stability. In addition, using a much shorter cavity length, it can achieve high spatial resolution and great reduction in temperature cross effects.
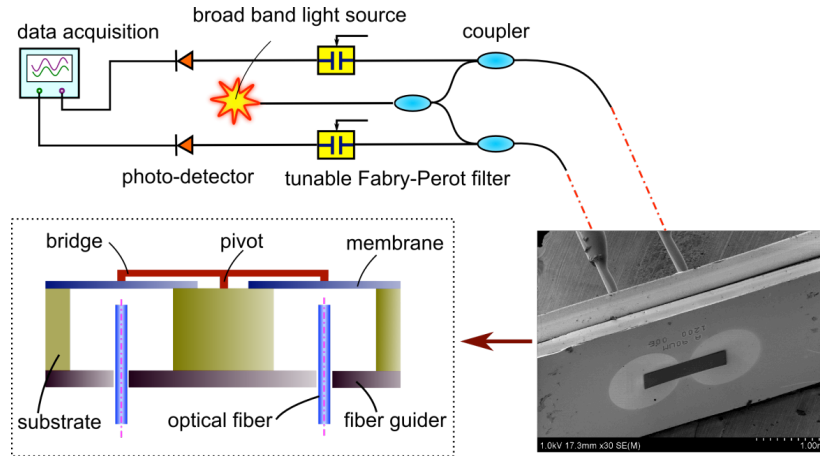

Figure 6: Low coherence fiber optic interferometer system for the mico-fabricated directional microphone.

To study of the performance of the MEMS device, the directional cues in terms of the *mIPD* are characterized with respect to the sound frequency and the sound azimuth. In Figure 7, it can be seen that *mIPD* can be amplified over a wide frequency range. By using a scanning laser vibrometer (Polytec MSA400), the rocking and bending modes (see the mode shapes shown in **Figure 7**) are obtained to be at 10.3 kHz and 29.5 kHz, close to the design values. Furthermore, the *mIPD* is seen to achieve its maximum value and experience a sign change at the rocking natural frequency, while at the bending natural frequency, the mIPD is close to zero. At the working of 8 kHz, the experimental value of *mIPD* is

clearly a linear function of θ in the range of -30°≤θ≤30° (see inset of **Figure 7**), and the slope of the linear range, DS, is estimated to be 3.29 deg/deg, which is 18.3 times of the initial value of the IPD (0.18deg/deg) at the midline without amplification. Such a performance is equivalent to that can be obtained from a conventional microphone pair with a separation of 22.9 mm (18 times larger than that of the fly-ear sized sensor). The experimental results compare well with the simulation results obtained on the basis of a 2DOF model.

It is mentioned that the damping factors of the device are determined to be 0.10 and 0.15, which are much smaller than those of the fly ear. Although it is difficult to realize the damping characteristics of the fly ear in MEMS devices, smaller damping factors render a higher amplification of the directional sensitivity DS (designed value: 1.18 deg/deg and the experimental value: 3.29deg/deg), which can help increase the signal-to-noise ratio for sound localization.
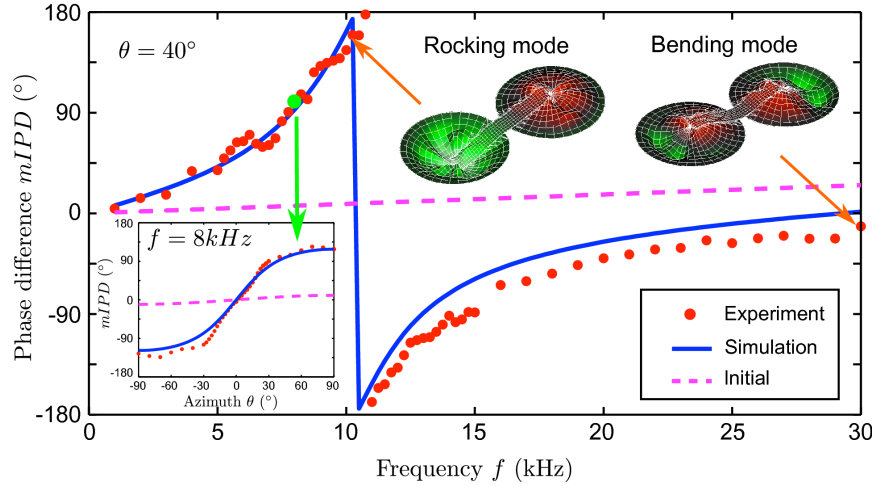

Figure 7: Directional cue *mIPD* as a function of sound frequency for the fabricated bio-inspired device. The mode shapes of the rocking mode (10.3 kHz) and the bending mode (29.5 kHz) obtained from laser Doppler vibrometer tests are also shown. The simulation results are obtained by using damping factors of 0.10 and 0.15. The initial phase difference refers to the acoustic inputs. At the working frequency 8 kHz, the measured *mIPD* has a linear relationship with θ from -30° to 30°. DS for this linear azimuth range is 3.29 deg/deg, 18.3 times the initial DS at the midline of 0.18 deg/deg.

C. Development Miniature Optical Detection and Signal Processing System

As discussed previously, optical detection technique has been used to interrogate the fly-ear inspired sensors. However, even with a miniature size of the sensor itself, the large scale optical system greatly hinders the application of the fly-ear inspired sensors. In this work, the untapped potential of a low coherence optical sensor system is explored to develop a Micro-Opto-Electro-Mechnical-System (MOEMS) sensor platform that is capable of integrating multiplexed Fabry-Perot (FP) interferometer based sensors. A schematic of the proposed differential low coherence interferometer based sensing element module with all of the components and waveguide integrated on a single MOEMS chip is shown in **Figure 8**. Light from a low coherence light source with a coherence length L_c is first sent to the reference interferometer – a tunable Fabry-Perot interferometer, and then via a waveguide splitter to two combiners. At the output of each combiner, the light beam (E_{in1} or E_{in2}) is sent to the sensor interferometer – a Fabry-Perot interferometer based sensor. A Fabry-Perot configuration uses two mirrors (a partial mirror and a second mirror, which can be either a partial or a complete mirror) to form a cavity. The reflected light waves from the mirrors (e.g., $E_{out2} = E_{out21} + E_{out22}$) will have an optical path difference (OPD) L_s that induces a phase difference $\phi_s = k_0 L_s$, where $k_0 = 2\pi/\lambda$ is the free-space wave number and λ is the
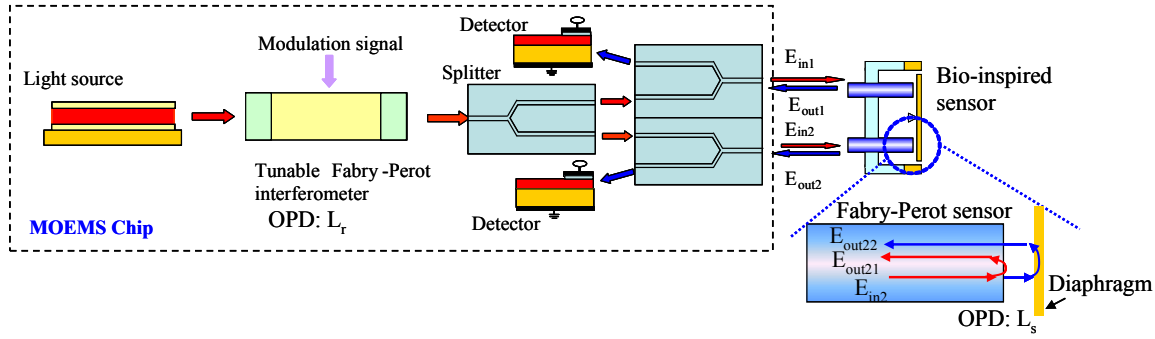
Figure 8: Schematic of low coherence interferometer based MOEMS chip integrated with biology-inspired sensor.

wavelength. The acoustic pressure induced diaphragm deflection produces a phase difference change $\Delta\phi$ in ϕ_s. The reflected light from each Fabry-Perot sensor is then coupled back to the waveguide and sent to a photodetector. The on-chip tunable Fabry-Perot interferometer, which has an initial optical path difference L_r (or phase difference $\phi_r = k_0 L_r$), acts as a reference interferometer. When it is path-matched to the Fabry-Perot sensor ($L_r \cong L_s$) and the coherence length $L_c \ll L_r$, L_s, the output intensity received by the detector is

$$I_{out} \approx I_{dc} + I_{ac} \cos k_0 (L_s - L_r) = I_{dc} + I_{ac} \cos(\phi_s - \phi_r) = I_{dc} + I_{ac} \cos(\Delta\phi),$$

where A and B are the constants related to the mirror properties of the FP interferometer, and $\Delta\phi$ is the differential phase change between the sensing interferometer and reference interferometer. Note that $\Delta\phi$ is the only parameter related to the center displacement (X) of the biology-inspired diaphragm and $\Delta\phi = 2k_0 X$. Therefore, the pressure sensitivity (displacement/pressure) of the diaphragm can be amplified by a factor of $2k_0$ (10^7 times at $\lambda = 1300$ nm). Such high sensitivity enables the detection of a sound pressure level of 10 dB (the sound level of calm breathing). In addition, owing to the differentiation of the phase signal between the two interferometers, this technique has immunity to wavelength and power fluctuation induced noise, permits a short effective sensing cavity (several μm), and yields a high resolution ($\sim 10^{-4}$ nm[5]) and a large dynamic range (several tens of wavelength). This is the first attempt towards developing a low coherence interferometer based MOEMS detection system.

An optical Micro-Electro-Mechanical-System (MEMS) sensor platform was developed for the miniature fiber optic microphones. The key components of this platform include a superluminescent diode (SLED), photodetector chips, and a MEMS tunable Fabry-Perot (FP) filter. The working principle of the multi-functional sensor platform is based on a *differential* low coherence interferometer consisting of multiple sensing interferometers (multiple sensors) and a single reference interferometer (the FP filter). By measuring the differential phase signal between the reference interferometer and each of the reference interferometers, this platform has immunity to wavelength and power fluctuation induced noise, permits a short effective sensing cavity, and yields a high resolution and a large dynamic range.

The key components of the optical MEMS platform are shown in **Figure 9**. The SLED can emit a broadband light with a center wavelength of 1310 nm (coherent length 35 μm) and a power of 120 μW at 100 mA. The tunable FP filter is formed between a fiber endface and a curved MEMS mirror driven by a comb drive, which has a cavity length of 60 μm. The comb drive is designed to have a resonant frequency of 1.4 kHz. The photodiode has a receiving area of 300 μm in diameter and a responsivity of 0.9 A/W at 1310 nm.
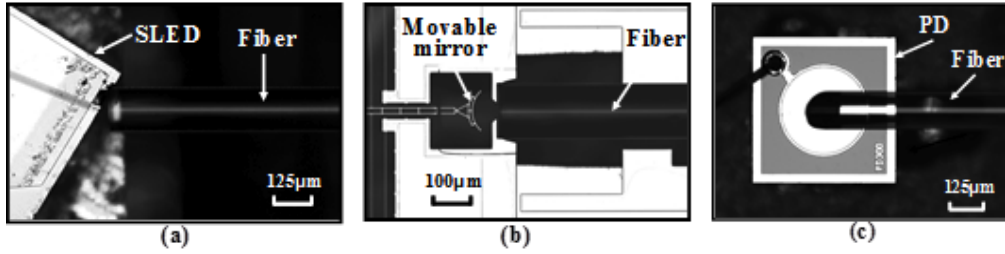
Figure 9: Close-ups of key components of the optical sensor board in the MEMS platform: (a) SLED; (b) Tunable Fabry-Pérot filter; (c) photodiode.

Finally, we have integrated the MOEMS on-chip optical system with a wireless transceiver system to realize a fully functional, inexpensive and portable sensor system. The final prototype of wireless optical signal processing system is shown in **Figure 10**.
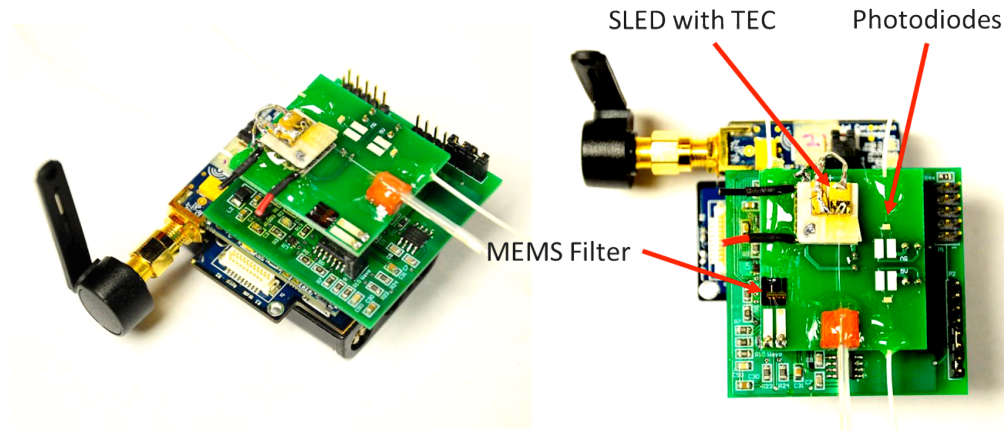.

Figure 10: Integrated optical detection and signal processing chip

D. Bio-Inspired Sound Localization with Fly-Ear Inspired Sensors

A bio-inspired sound localization scheme was developed, which is based on the fly's unique localization/lateralization scheme. We further implemented this sound localization scheme on a motorized control platform by using the fly-ear inspired sensors described in the previous section.

Inspired by the fly's unique localization/lateralization scheme for sound source localization, a bio-inspired localization scheme is developed and implemented by controlling of a motorized platform. As shown in **Figure 11**, this platform consists of two motorized one dimensional rotational stages (Newport URS75BPP), with one stage stacked on top of the other. The bio-inspired MEMS acoustic sensor discussed in the previous quarterly report was mounted on the tip of a homemade fixture. A speaker (ESS AMT) was used as the sound source. The centers of both stages were aligned vertically with the sensor by manual adjustment.

The bio-inspired MEMS directional microphone uses the low coherence fiber optic interferometer (LCFOI) system (see **Figure 6**) to detect the displacement of the two membrane centers. The two motorized stages are connected to and controlled by a motion controller (Newport ESP300). The outputs of the photo-detectors are connected to a data acquisition board (NI USB-6259). Both the motion controller and the data acquisition board are connected to a laptop with the localization algorithm implemented in a Labview program.
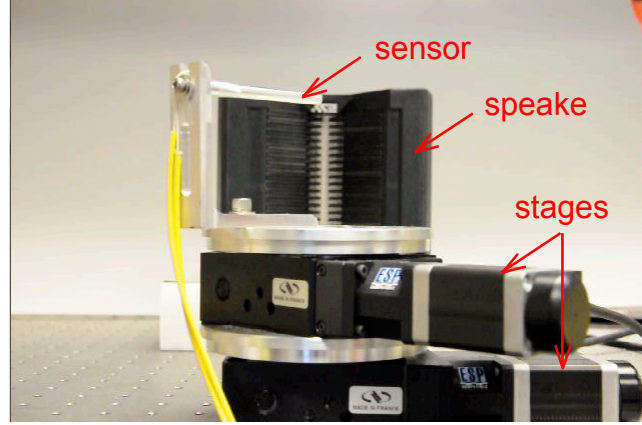
Figure 11: Control platform using two rotational stages and integrated with a bio-inspired MEMS directional microphone.

First, the phase difference mIPD of the MEMS device is measured at various azimuth angles when a 7kHz pure tone (close to the optimal working frequency of the sensor) is played through the speaker. The mechanical interaural time difference (mITD) is calculated by finding the maximum of the cross-correlation of the two time signals for the two membranes

$$mITD = \arg corr\left(W_l, W_r\right) \tag{11}$$

which is converted to phase difference mIPD. As shown in Error! Reference source not found., mIPD is a linear function of azimuth in the range of -30°≤θ≤30°. By approximating their relationship in the linear range by a straight line, the directional sensitivity is calibrated as 1.32, which is 8.6 times the directional sensitivity using a conventional uncoupled configuration. It should be noted that there is a zero offset (5.09°) at the zero azimuth due to the unsynchronized data acquisition and alignment error. In short, the phase difference in the linear range is approximated by the following formula:

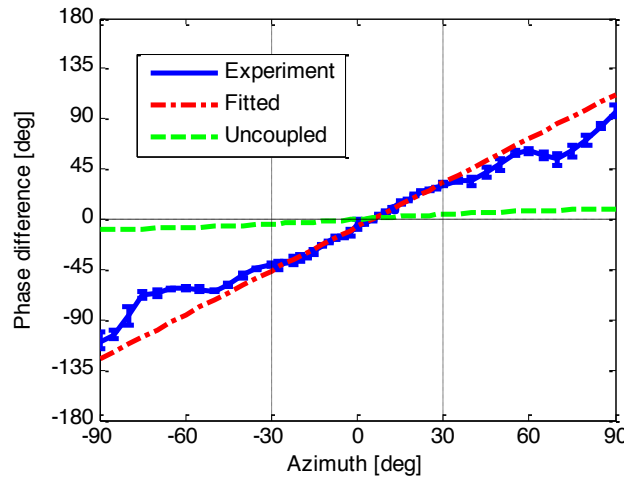$$mIPD = 1.32 \times \left(\theta - 5.09°\right). \tag{12}$$

Figure 12: Phase difference of the MEMS sensor as a function of azimuth at 7kHz. The uncoupled case corresponds to a conventional directional microphone setup without the mechanical coupling.

Upon receiving two signals of the membranes, the control program first calculates the phase difference mIPD. Then, an azimuth estimate is obtained by using the following formula:

$$\tilde{\theta} = \frac{mIPD}{1.32} + 5.09°.$$ (13)

If the estimate is beyond the linear range (e.g. 45°), the control program moves the sensor toward the end position of the linear range (e.g. 30°). Once the source is within the linear range, the sensor will be moved to that specific location so that it will point to the source. This scheme is essentially the same as the fly's localization/lateralization scheme.

As a demonstration of the bio-inspired localization scheme, the sensor is placed at 80° initially (speaker stage reading of 0° and sensor stage reading of 80°), as shown in **Figure 13**. As the sensor pinpoints the source (both stage readings are 0°), the speaker stage starts to move randomly in either direction. However, the control program is able to detect the random motion of the source and move the sensor stage in the opposite direction so that the sensor is maintained to be able to still pinpoint the source.
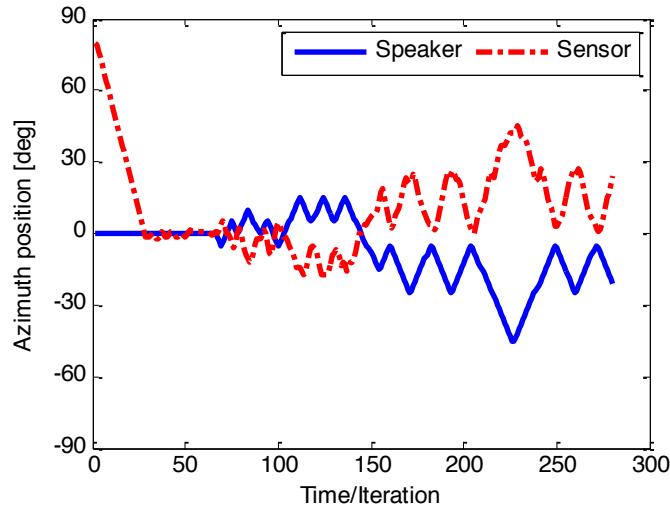

Figure 13: Real time speaker and sensor position readings from the motorized stages. At about 70 interactions, a command is sent to the speaker stage to move randomly in either direction and the movement step increases with time.

In **Figure 14**, the actual position of the source relative to the sensor is compared to that of the estimate value from the localization system. In the beginning stage, the source is out of the linear range, which is equivalent to 30° for the sensor. Once the source is within the linear range, the sensor is able to locate the source and track its position even when the source is moving in a random fashion. This experiment successfully demonstrates the application of fly-ear localization/lateralization scheme in one dimensional sound source localization and tracking.
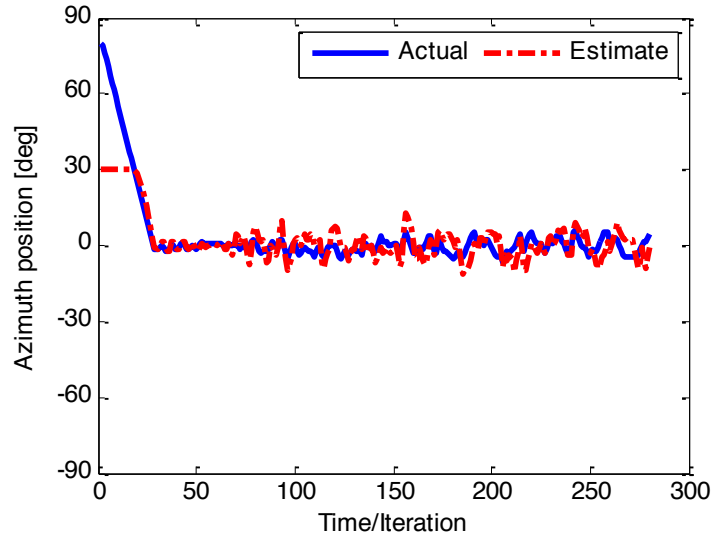
Figure 14: Time history of actual and estimated positions of the sound source.

E. Investigation of Optimal Control in Fly's Localization Scheme

The parasitic fly *Ormia ochracea* has been found to have superacute directional hearing, although its distance between auditory organs is only half millimeter. In addition, the fly employs a unique localization/lateralization scheme to locate its host crickets: the fly estimates the true position of the sound source in the linear range of azimuth up to 20-30deg, whereas it only makes a left/right decision when the source is beyond this linear range.

We previously showed that this scheme may relate to the characteristics of its directional sensitivity (DS) of its mechanically coupled eardrums. At its working frequency 5kHz, which is the calling song frequency of male crickets, DS is not only flat in the vicinity of midline (azimuth up to 30deg), but also higher than what is achievable at any other frequencies. Based on this, an argument is made that the fly ear represents a nature designed optimal structure.

The goal of the study in this section is to investigate the fly ear phenomena another angle, from the perspective of optimal control. By modeling in 1D (azimuth), the optimal control problem is first described, and its analytical solution is obtained. Then efforts are made to explore the relationship between the fly's localization/lateralization scheme and the phase portrait of the optimal control solution.

Description of optimal control problem

- *Model (bearing-only 1D control problem)*

Assuming the state variables are the bearing angle and the rotational speed: $x_1 = \theta, x_2 = \dot{\theta}$, the state equations can be written as:

$$\begin{cases} \dot{x}_1 = x_2 \\ \dot{x}_2 = u - \mu x_2 \end{cases}, \tag{14}$$

where u is the control moment, μx_2 is the dragging force that is assume to be proportional to the rotational speed.

Another assumption is on the control moment, which is subject to the constraint:

$$|u| \le 1. \tag{15}$$

This constraint limits the maximum control the fly can apply. As a result, the maximal speed is equal to $1/\mu$.

In matrix form, (14) can be written as:

$$\dot{\mathbf{X}} = \mathbf{A}\mathbf{X} + \mathbf{B}u, \tag{16}$$

where

$$\mathbf{X} = \left\{ \begin{array}{c} \dot{x}_1 \\ \dot{x}_2 \end{array} \right\}, \tag{17}$$

$$\mathbf{A} = \begin{bmatrix} 0 & 1 \\ 0 & -\mu \end{bmatrix}, \tag{18}$$

$$\mathbf{B} = \begin{bmatrix} 0 \\ 1 \end{bmatrix}. \tag{19}$$

Since the controllability matrix has full rank, this system is fully controllable.

- **_Solution of state equation_**

$$\left[s\mathbf{I} - \mathbf{A} \right]^{-1} = \begin{bmatrix} s & -1 \\ 0 & s+\mu \end{bmatrix}^{-1} = \begin{bmatrix} \dfrac{1}{s} & \dfrac{1}{s(s+\mu)} \\ 0 & \dfrac{1}{s+\mu} \end{bmatrix} \tag{20}$$

Taking the inverse Laplace transform of (20), we can obtain the transition matrix:

$$e^{\mathbf{A}t} = \begin{bmatrix} 1 & \dfrac{1}{\mu}\left(1 - e^{-\mu t}\right) \\ 0 & e^{-\mu t} \end{bmatrix}. \tag{21}$$

Therefore, the state at any time t is

$$\mathbf{X}(t) = e^{\mathbf{A}t}\mathbf{X}(0) + \int_0^t e^{\mathbf{A}(t-\tau)}\mathbf{B}u(\tau)d\tau$$

$$= \begin{bmatrix} 1 & \dfrac{1}{\mu}\left(1 - e^{-\mu t}\right) \\ 0 & e^{-\mu t} \end{bmatrix} \mathbf{X}(0) + \int_0^t \begin{bmatrix} \dfrac{1}{\mu}\left(1 - e^{-\mu(t-\tau)}\right) \\ e^{-\mu(t-\tau)} \end{bmatrix} u(\tau)d\tau . \tag{22}$$

If the control u is constant in the interval $\left[t, t+\Delta T\right]$, the state at the end of the interval is related to the state in the beginning of the interval by:

$$\mathbf{X}(t + \Delta T) = \mathbf{A}^{\Delta T}\mathbf{X}(t) + \mathbf{B}^{\Delta T}u, \tag{23}$$

where

$$\mathbf{A}^{\Delta T} = \begin{bmatrix} 1 & \dfrac{1}{\mu}\left(1 - e^{-\mu\Delta T}\right) \\ 0 & e^{-\mu\Delta T} \end{bmatrix}, \tag{24}$$

$$\mathbf{B}^{\Delta T} = \begin{bmatrix} \dfrac{1}{\mu}\Delta T - \dfrac{1}{\mu^2}\left(1 - e^{-\mu\Delta T}\right) \\[3ex] \dfrac{1}{\mu}\left(1 - e^{-\mu\Delta T}\right) \end{bmatrix}. \tag{25}$$

The above equation is helpful for the numerical implementation in Matlab.

- *Performance measure*

The control problem here is to move from any initial state to the final rest state, $\mathbf{x} = \mathbf{0}$. To get the optimal control, we need a general form of performance cost:

$$J(u) = \int_{t_0}^{t_f} \left[\lambda + |u(t)|\right] dt, \tag{26}$$

which is a weighted sum of elapsed time and control effort (or consumed fuel). The goal is to find the optimal control that minimizes the performance cost J. If λ is equal to zero, J reduces to control effort only; When λ is zero, the goal is simply to minimize the travel time.

For the optimal control problem formulated above, an analytical solution can be obtained by using Pontryagin's minimum principle[6], as follows.

Solution of the optimal control problem

The Hamiltonian can be written as:

$$\begin{aligned} H &= \lambda + |u(t)| + p_1(t)x_2(t) + p_2(t)\left[u(t) - \mu x_2(t)\right] \\ &= |u(t)| + p_2(t)u(t) + \lambda + p_1(t)x_2(t) - \mu p_2(t)x_2(t) \end{aligned} \tag{27}$$

where p_1, p_2 are the co-state variables.

The co-state equations are:

$$\begin{cases} \dot{p}_1^*(t) = -\dfrac{\partial H}{\partial x_1} = 0 \\[3ex] \dot{p}_2^*(t) = -\dfrac{\partial H}{\partial x_2} = -p_1^*(t) + p_2^*(t)\mu = 0 \end{cases}, \tag{28}$$

The solutions of the co-state are:

$$\begin{cases} p_1^*(t) = c_1 \\[2ex] p_2^*(t) = \dfrac{c_1}{\mu} + c_2 e^{\mu t} \end{cases} \tag{29}$$

For the optimal control $u^*(t)$, we have the following relationship from the Pontryagin's minimum principle:

$$|u^*(t)| + p_2^*(t)u^*(t) \le |u(t)| + p_2^*(t)u(t). \tag{30}$$

We only need to choose the control to minimize the LHS of (30).

Depending on the value of p_2^*, the control u can be take one of the three values:

$$u^*(t) = \begin{cases} -1 & p_2^* > 1 \\ 0 & -1 < p_2^* < 1 \\ 1 & p_2^* < -1 \end{cases} \tag{31}$$

Apparently, the trajectory can not end with a segment with $u^* = 0$. Also notice that p_2^* in (29) is a monotonically changing function of time t, which means u^* can not change abruptly from 1 to -1, or vice versa. Therefore, candidates for the control history are:

    (1) End with a $u = -1$ segment: $\{-1\}, \{0 \rightarrow -1\}, \{1 \rightarrow 0 \rightarrow -1\}$;

    (2) End with a $u = 1$ segment: $\{1\}, \{0 \rightarrow 1\}, \{-1 \rightarrow 0 \rightarrow 1\}$.

However, $\{-1\}$ and $\{0 \rightarrow -1\}$ can be considered as a portion or a special case of $\{1 \rightarrow 0 \rightarrow -1\}$, and $\{1\}$ and $\{0 \rightarrow 1\}$ can be considered as a portion of $\{-1 \rightarrow 0 \rightarrow 1\}$. Therefore, we only need to consider two control scenarios: $\{1 \rightarrow 0 \rightarrow -1\}$ and $\{-1 \rightarrow 0 \rightarrow 1\}$. Starting from the final zero state, we calculate the state set at which the control makes the switch.

- **Case 1: $\{-1 \rightarrow 0 \rightarrow 1\}$**

Assume the control u switches from -1 to 0 at t_1, and from 0 to 1 at t_2, and the state reaches the zero state at t_f.

(1) Segment $t_2 \leq t \leq t_f : u = 1$

From (22), we have

$$\begin{cases} x_1(t_f) = x_1(t_2) + \dfrac{1}{\mu} x_2(t_2)\left[1 - e^{-\mu(t_f - t_2)}\right] - \dfrac{1}{\mu^2} + \dfrac{1}{\mu}(t_f - t_2) + \dfrac{1}{\mu^2} e^{-\mu(t_f - t_2)} = 0 \\ x_2(t_f) = x_2(t_2) e^{-\mu(t_f - t_2)} + \dfrac{1}{\mu}\left[1 - e^{-\mu(t_f - t_2)}\right] = 0 \end{cases} \quad (32)$$

Solving (32) gives:

$$\begin{cases} x_1(t_2) = -\dfrac{1}{\mu}(t_f - t_2) - \dfrac{1}{\mu^2}\left[1 - e^{\mu(t_f - t_2)}\right] \\ x_2(t_2) = \dfrac{1}{\mu}\left[1 - e^{\mu(t_f - t_2)}\right] \end{cases} \quad (33)$$

Therefore, the state lies on this curve:

$$x_1(t_2) = -\dfrac{1}{\mu^2} \ln\left[1 - \mu x_2(t_2)\right] - \dfrac{1}{\mu} x_2(t_2) \quad (34)$$

where $x_1(t_2) \geq 0$ and $x_2(t_2) \leq 0$, since $\mu > 0$ and $t_f \geq t_2$.

(2) Segment $t_1 \leq t \leq t_2 : u = 0$

From (22), we have:

$$\begin{cases} x_1(t_2) = x_1(t_1) + \dfrac{1}{\mu} x_2(t_1)\left[1 - e^{-\mu(t_2 - t_1)}\right] \\ x_2(t_2) = x_2(t_1) e^{-\mu(t_2 - t_1)} \end{cases} \quad (35)$$

At t_1, $u^*(t_1) \leq 0$, $p_2^*(t_1) = 1$

$$\frac{c_1}{\mu} + c_2 e^{\mu t_1} = 1, \tag{36}$$

$$H(t_1) = \lambda + p_1(t_1)x_2(t_1) - \mu x_2(t_1) = \lambda + c_1 x_2(t_1) - \mu x_2(t_1) = 0. \tag{37}$$

At t_2, $u^*(t_2) \geq 0$, $p_2^*(t_2) = -1$

$$\frac{c_1}{\mu} + c_2 e^{\mu t_2} = -1, \tag{38}$$

$$H(t_2) = \lambda + p_1(t_2)x_2(t_2) + \mu x_2(t_2) = \lambda + c_1 x_2(t_2) + \mu x_2(t_2) = 0. \tag{39}$$

From (36) and (38), we can obtain the difference $t_2 - t_1$:

$$t_2 - t_1 = \frac{1}{\mu} \ln \frac{c_1 + \mu}{c_1 - \mu}. \tag{40}$$

The constant c_1 can be solved from (37):

$$c_1 = \mu - \frac{\lambda}{x_2(t_1)}. \tag{41}$$

Substitute c_1 in (40) using (41):

$$t_2 - t_1 = \frac{1}{\mu} \ln \left[1 - \frac{2\mu}{\lambda} x_2(t_1) \right]. \tag{42}$$

Substituting (42) into (35), we can express the state at t_2 by the state at t_1:

$$\begin{cases} x_1(t_2) = x_1(t_1) - \dfrac{2x_2^2(t_1)}{\lambda - 2\mu x_2(t_1)} \\ x_2(t_2) = x_2(t_1) \dfrac{\lambda}{\lambda - 2\mu x_2(t_1)} \end{cases}. \tag{43}$$

Apparently, $\begin{bmatrix} x_1(t_2) & x_2(t_2) \end{bmatrix}^T$ is on the trajectory of (34):

$$x_1(t_1) = -\frac{1}{\mu} x_2(t_1) - \frac{1}{\mu^2} \ln \left[1 - \frac{\mu \lambda x_2(t_1)}{\lambda - 2\mu x_2(t_1)} \right], \tag{44}$$

Where $x_1(t_1) \geq 0$ and $x_2(t_1) \leq 0$.

- **Case 2: $\{1 \to 0 \to -1\}$**

Assume the control u switches from 1 to 0 at t_1, and from 0 to -1 at t_2, and the state reaches the zero state at t_f.

(1) Segment $t_2 \leq t \leq t_f$: $u = -1$

From (22), we have

$$\begin{cases} x_1(t_f) = x_1(t_2) + \dfrac{1}{\mu} x_2(t_2)\left[1 - e^{-\mu(t_f - t_2)}\right] + \dfrac{1}{\mu^2} - \dfrac{1}{\mu}(t_f - t_2) - \dfrac{1}{\mu^2} e^{-\mu(t_f - t_2)} = 0 \\ x_2(t_f) = x_2(t_2) e^{-\mu(t_f - t_2)} - \dfrac{1}{\mu}\left[1 - e^{-\mu(t_f - t_2)}\right] = 0 \end{cases}. \tag{45}$$

The switch from $u = 0$ to $u = -1$ occurs on this curve:

$$x_1(t_2) = \frac{1}{\mu^2} \ln\left[1 + \mu x_2(t_2)\right] - \frac{1}{\mu} x_2(t_2), \tag{46}$$

where $x_1(t_2) \le 0$ and $x_2(t_2) \ge 0$.

(2) Segment $t_1 \le t \le t_2$: $u = 0$

The switch from $u = 1$ to $u = 0$ occurs on this curve:

$$x_1(t_1) = -\frac{1}{\mu} x_2(t_1) + \frac{1}{\mu^2} \ln\left[1 + \frac{\mu \lambda x_2(t_1)}{\lambda + 2\mu x_2(t_1)}\right], \tag{47}$$

where $x_1(t_1) \le 0$ and $x_2(t_1) \ge 0$.

Results and discussion

Based on the solutions obtained in the previous section, the whole state can be split into four regions, as shown in **Figure 15**. Starting from an initial state point A_1 in Region I (or A_2 in Region III), the control is $u = -1$ (or $u = 1$), till the state reaches the first switching interface OB_1 (or OB_2), after which the control is turned off, i.e. $u = 0$, in Region II (or Region IV). When the state approaches the second switching interface OC_1 (or OC_2), the control is again turned on, $u = 1$ (or $u = -1$). Finally, it reaches the final zero state O along OC_1 (or OC_2). According to the optimal control theory, since $A_1 \rightarrow B_1 \rightarrow C_1 \rightarrow O$ is the optimal trajectory starting from initial state at A_1, $B1 \rightarrow C_1 \rightarrow O$ is also optimal if the trajectory is initiated at B_1.
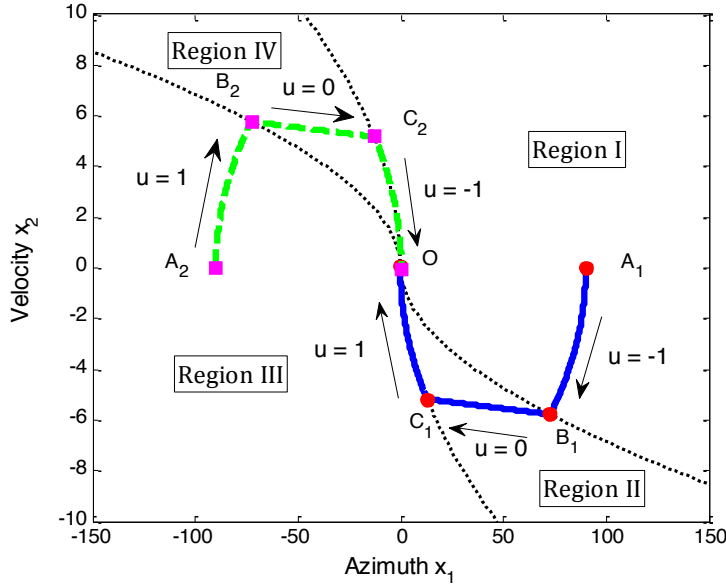

Figure 15: Exemplary optimal trajectories ($\lambda = 1, \mu = 0.01$), in which the initial state is at A_1 ($x_1 = 90, x_2 = 0$) or A_2 ($x_1 = -90, x_2 = 0$), and the final state is at the origin O.

Figure 16 shows the time history of the trajectory $A_1 \rightarrow B_1 \rightarrow C_1 \rightarrow O$ in Figure 15. Starting from $x_1 = 90, x_2 = 0$, a maximum control is applied ($u = -1$) to accelerate toward the final position $x_1 = 0$. After coasting in the middle segment of the trajectory, the system is controlled by a deceleration force $u = 1$ to reach the final position with zero velocity.
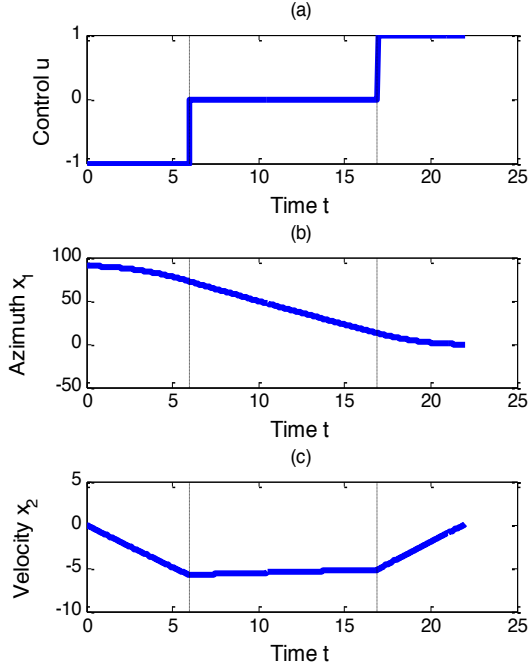
Figure 16: Time history of the trajectory $A_1 \rightarrow B_1 \rightarrow C_1 \rightarrow O$ in Figure 15 ($\lambda = 1, \mu = 0.01$). (a) control, (b) azimuth, and (c) velocity.
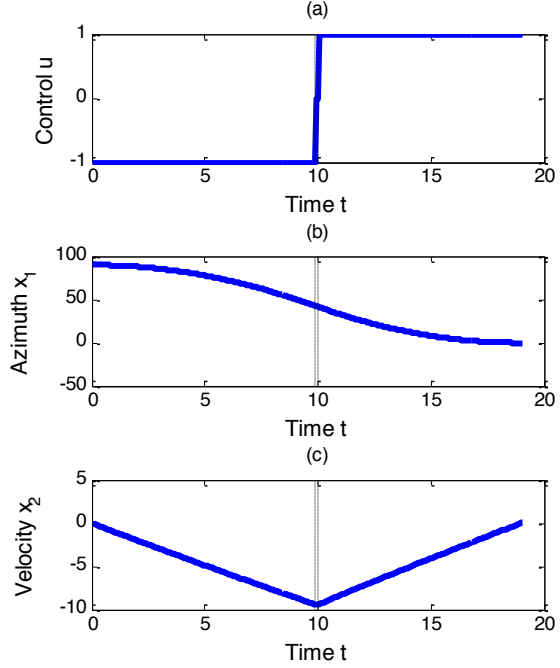
Figure 17: Time history of the trajectory starting from $x_1 = 90, x_2 = 0$. (a) control, (b) azimuth, and (c) velocity. The parameters of the performance measure are changed to $\lambda = 100, \mu = 0.01$.

The length of the coasting segment varies depending on the relative priority of time and control effort in the performance measure in (26), which is controlled by the parameter λ. Increasing λ from 1 to 100 means it is more of a priority to reduce the travel time. The time history in Figure 17 shows that the total travel time is reduced from 22 for λ=1 to 19 for λ=100. However, this reduction is at the expense of increasing control effort. Excluding the coasting time, the time for u=±1 instead increases from 11 for λ=1 to 19 for λ=100.

Revisit of localization/lateralization scheme of the fly ear

In the phonotactic experiment on the fly[4], it is found that the fly's turning speed is a sigmoid function of the speaker azimuth, as shown in **Figure 18**. The fly employs a localization/lateralization scheme to accurately locate its host crickets, i.e. the fly estimates the true position of the source when the source is within the linear range (azimuth up to 20-30°), and otherwise it only makes a left or right decision and turns a maximal angle toward the source.

This unique scheme is related to the fly's sensing mechanism. By looking at the directional sensitivity (DS, defined as the first derivative of mechanical interaural phase difference *mIPD* with respect to azimuth θ), as shown in Error! Reference source not found., we can find out that in the vicinity of midline (-30°≤θ≤30°), DS is not only very flat at the fly's working frequency 5kHz, but it is higher than what is achievable at any other frequency. In other words, if we use a straight line to approximate *mIPD* in the azimuth range -30°≤θ≤30°, the linearity is best at 5kHz, and the slope is maximal. The localization/lateralization scheme takes full advantage of the linear range so that the fly can accurately pinpoint the crickets.
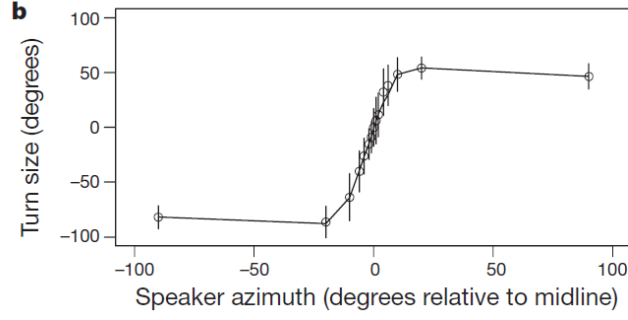
Figure 18: Fly's turning size measured in 1.2 seconds (equivalent to turn speed) as function of speaker azimuth (Mason et al, 2001).

In **Figure 19**, the phase portrait is obtained by using $\lambda = 100, \mu = 0.1$, which means the maximum speed achievable is $1/\mu = 10$. The resulting velocity-azimuth relationship is very similar to the sigmoid relationship in **Figure 18**, except the different orientations of the Z-shape. This is simply due to the fact that the reference is the fly in the phonotactic experiment, while the reference is the fixed speaker in the current simulation. In both cases, the head front ends up facing the speaker.
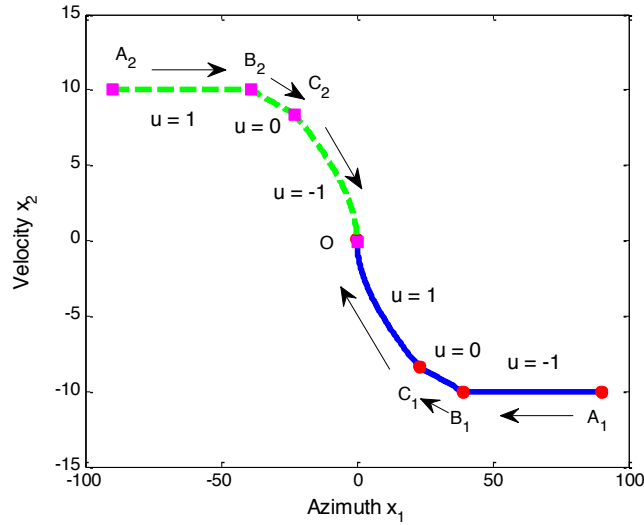

Figure 19: Phase portrait for the 1D system with optimal control for initial state at A$_1$(90,-10) or A$_2$(-90,10). The parameters for the optimal measures are $\lambda = 100, \mu = 0.1$.

Inspired by the fly's localization/lateralization scheme, we try to investigate how to design a control that is close to the optimal control. Assuming the full state is observable, one example of closed-loop control is as follows:

$$u = \begin{cases} -1 & \theta > 30 \\ -0.5 \times \dfrac{x_1}{30} - 0.5\mu x_2 & -30 \le \theta \le 30 \\ 1 & \theta < -30 \end{cases} \tag{48}$$

where the control is still subject to the constraint $|u| \le 1$.

Figure 20 compares the results of the above defined closed-loop control with the optimal control. For the closed-loop control, the state overshoots the target: when x_1 reaches 0 for the first time at t=9.7, x_2 is equal to -6.38. Although it settles downs in the end, it takes 68.7 time to get to the zero state, much longer than 13 by the optimal control. Also, the control effort (defined as $\int |u| dt$) is 29.6% more (14.58 as opposed to 11.25).

Note that in the beginning, the feedback is based on the position x_1 only so that only the azimuth needs to be estimated. In this case, there is no additional damping introduced by the feedback; the real part of the closed-loop system is just -μ. Therefore, the system will take longer to settle down.
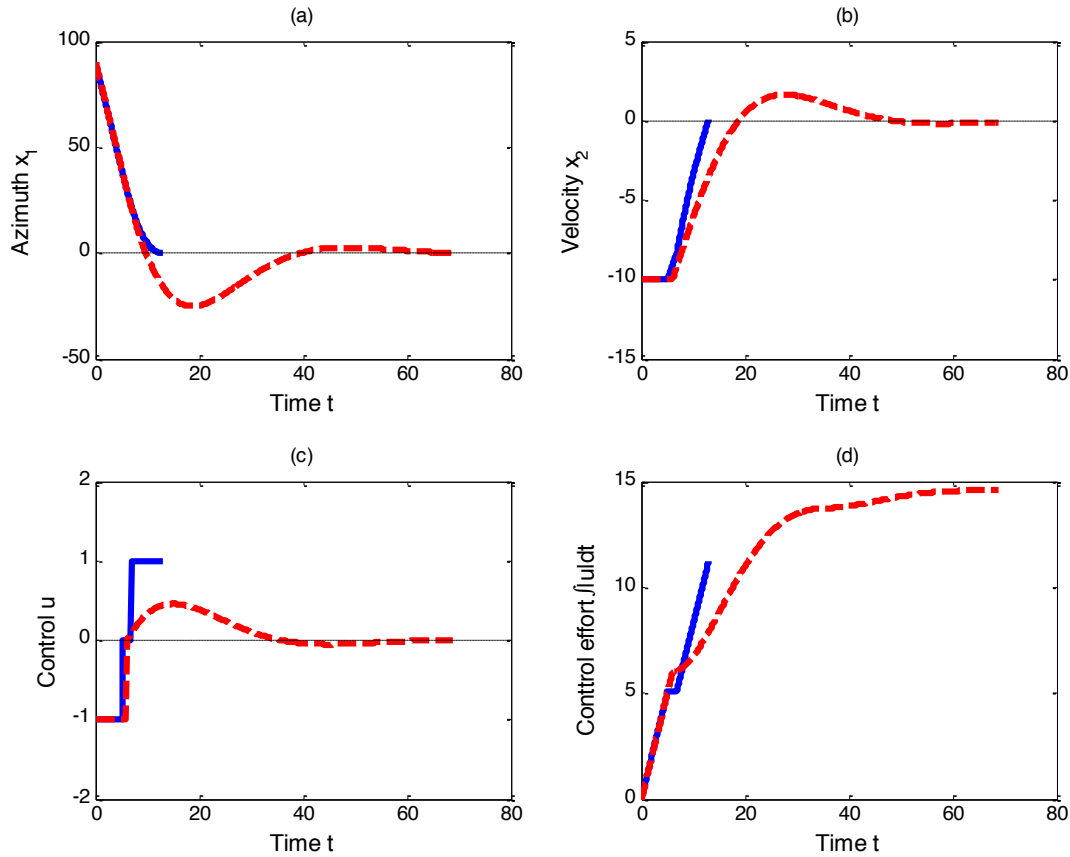

Figure 20: Comparison of the optimal control (blue solid line) and the closed-loop control (red dashed line) in (35).

III. List of Publications and Patent

Archived Journal Papers:

1) H. Liu, M. Yu, and X. M. Zhang, "Biomimetic optical directional microphone with structurally coupled diaphragms," Applied Physics Letters 93, 243902, 2008. (also selected for the January 1, 2009 issue of Virtual Journal of Biological Physics Research)
2) A. Lisiewshi, H. Liu, M. Yu, L. Currano, and D. Gee, "Fly-ear inspired micro-sensor for sound source localization in two dimensions," *Journal of Acoustic Society of America-Express Letters*, 129(5) pp. EL166-171, 2011.

Conference Papers:

1. H. Liu, M. Yu, L. Currano, and D. Gee, "Fly-ear inspired miniature directional microphones: modeling and experimental study," Proceedings of IMECE2009: 2009 ASME International Mechanical Engineering Congress and Exposition, Lake Buena, FL, Nov 13-Nov 19, 2009.

2. A. P. Lisiewski, H. Liu, and M. Yu, "FLY EAR INSPIRED MINIATURE SOUND SOURCE LOCALIZATION SENSOR: LOCALIZATION IN TWO DIMENSIONS," Proceedings of IMECE2010: 2010 ASME International Mechanical Engineering Congress and Exposition, Vancouver, BC, Nov 12-Nov 18, 2010.

3. H. Liu, Z. Chen, and M. Yu, "Bio-inspired acoustic sensors for sound source localization," *SPIE 2008 Symposium on Smart Structures and Materials*, San Diego, CA, March 2008.

4. H. Liu, X.M. Zhang, and M. Yu, "Understanding fly-ear inspired directional microphones," *SPIE 2009 Symposium on Smart Structures and Materials*, San Diego, CA, March 2009.

5. H. Liu, L Currano, and M. Yu, "Fly-ear inspired acoustic sensors for gunshot localization," *SPIE 2009 Symposium on Defense, Security, and Sensing*, Orlando, FL, April 2009.

6. H. Liu and M. Yu, "A novel approach to develop miniature directional microphones: bio-inspired mechanical coupling," *SPIE 2010 Symposium on Smart Structures and Materials*, San Diego, CA, March 2009.

7. H. Liu and M. Yu, "A new approach to tackle noise issue in miniature directional microphones: bio-inspired mechanical coupling," *SPIE 2010 Symposium on Smart Structures and Materials*, Proc. of SPIE, Vol. **7647**, 76470P, San Diego, CA, March 2010.

8. H. Liu and M. Yu, "Fly-ear inspired directional microphone: effects of air cavity," *SPIE 2011 Symposium on Smart Structures and Materials*, San Diego, CA, March, 2011.

Patent:

1. M. Yu and H. Liu, University of Maryland Invention Disclosure No. PS2010-23, Fly-Ear Inspired Miniature Acoustic Sensor System, filed in Feb. 2010. US Provisional Patent 61/313,461. Patent application filed in March 2011.

III. Personnel Supported

In addition to the PI, three graduate students were partially supported by this contract: Haijun Liu, Andrew Lisiewski, and Yuxiang Liu. Andrew's Master's thesis and Haijun's Ph.D. dissertation are related to this project. Their thesis abstracts are provided as follows.

Abstract (Andrew Lisiewski)
A micro-scale sound localization sensor is developed and studied in this thesis to address the fundamental challenge of miniaturizing sound localization systems. When miniaturizing a microphone array there is a critical size limitation at which the array will be unable to localize the sound source in a discernible manner. However, a solution to this dilemma came about when studying the hearing mechanisms of a particular fly, known as *Ormia ochracea*. Background research into the hearing mechanisms of the fly found that it can accurately locate a sound source even though its eardrums are separated by a distance of only 500 μm. The fly's exceptional directional hearing capability has been linked to a distinct mechanical coupling between its two eardrums, which helps amplify minute directional cues. Inspired by the remarkable hearing capabilities of the fly's micro-scale ear, researchers have sought to develop micro-scale sensors to mimic the fly's ear. One limitation of simply imitating the fly's ear is that the fly is only capable of localizing a sound source in one dimension. In this thesis work, the knowledge gained from understanding the fly ear mechanism is applied to achieve the goal of developing a micro-scale sound

localization sensor capable of sound source localization in two dimensions. In this thesis, for the first time, micro-scale fly-ear inspired sensor devices employing three or four coupled membranes have been designed. Reduced-order models have been developed to achieve a fundamental understanding of the performance of each sensor design. Furthermore, a micro-scale sensor device incorporating three mechanically coupled membranes arranged in an equilateral triangular configuration has been successfully developed. Experimental study of the sensor device incorporated with a low coherence fiber optic interferometric detection system has suggested that the micro-scale fly-ear inspired sensor can achieve a much improved performance in terms of phase differences and directional cues when compared to a similar sized microphone array constructed with separate microphones. In addition, localization techniques have been developed to best use the fly-ear inspired sound localization sensors. Future work is suggested to incorporate this sensor system with a fully autonomous robot to improve robot homing and navigation.

Andrew Lisiewski has received his Master's degree in Spring 2011.

Abstract(Haijun Liu)

Microphone arrays have been widely used in sound source localization for many applications including hearing aid devices, robot navigation, and underwater sensor networks. In order to locate the sound in a discernible manner, the separation between microphones needs to be greater than a critical distance, which poses a fundamental challenge for the miniaturization of directional microphones. In nature, the auditory organs of the parasitoid fly *Ormia ochracea* are forcibly set close to each other (about 500 µm), but it can localize its cricket hosts with a resolution of as small as 2°. The key to this remarkable directional hearing is that the two tympana (ear drums) are coupled by a cuticular bridge that is pivoted about its center. Due to such mechanical coupling mechanism, the time difference is amplified by more than 30 times, and the best intensity difference can reach 10 dB. This innovative solution in nature can inspire one to find alternative approaches to developing miniature directional microphones.

The overall goal of this dissertation work is to unravel the underlying physics of the fly ear hearing mechanisms, and to apply this understanding to develop novel bio-inspired miniature directional microphones. In the first step of this proposed work, the fly ear's localization performance will be investigated based on an equivalent two-degrees-of-freedom model. Secondly, a novel bio-inspired directional microphone design with mechanically coupled diaphragms will be proposed to capture the essential dynamics of the fly ear. For this design, a non-dimensionalized continuum mechanics model will be developed. Parametric studies will be carried out to explore how the key normalized parameters affect the performance of this directional microphone. Such non-dimensionalization makes the analysis independent of the physical size, large or small. Next, this mechanics model will be used to guide the development of large-scale proof-of-concept microphones, which will be experimentally studied by using a low-coherence fiber optic interferometric detection system. Finally, miniaturization efforts will be made to develop microscale devices by using micro-fabrication techniques along with an on-chip integrated optical detection system.

It is expected that this dissertation work will provide physical insights into the fly ear mechanism and sound localization physics. The developed bio-inspired miniature directional microphone would significantly improve the localization performance while bringing down the size limit as imposed on the traditional sensors. As such, it would pave the way to new applications that have constrained space but require high sensitivity.

Haijun Liu is expected to defend his Ph.D. dissertation in late Spring 2012.

Yuxiang Liu has worked on the optical detection part of the project, whose dissertation was on a different topic. He received his Ph.D. in Fall 2010.

References

1 Miles, R., Robert, D. & Hoy, R. Mechanically coupled ears for directional hearing in the parasitoid fly Ormia ochracea. *Journal of the Acoustical Society of America* **98**, 3059-3070 (1995).

2 Meirovitch, L. *Fundamentals of Vibrations*. (McGraw-Hill, 2001).

3 Yovel, Y., Falk, B., Moss, C. & Ulanovsky, N. Optimal Localization by Pointing Off Axis. *Science* **327**, 701-704 (2010).

4 Mason, A., Oshinsky, M. & Hoy, R. Hyperacute directional hearing in a microscale auditory system. *Nature* **410**, 686-690 (2001).

5. Yao, Y. J. and Jackson, D.A., Principles of fiber-optic interferometry, in Optic sensor technology: fundamentals, edited by Grattan K.T.V. and Meggitt, B.T., Kluwer Academic Publishers, (2000).

6 Donald E. Kirk. *Optimal control theory: an introduction*. Dover, 2004.